# Understanding the Exfoliation and Dispersion of Hexagonal Boron Nitride Nanosheets by Surfactants: Implications for Antibacterial and Thermally Resistant Coatings

Ashleigh D. Smith McWilliams<sup>†,a</sup>, Cecilia Martínez-Jiménez<sup>†,a</sup>, Asia Matatyaho Ya'akobi<sup>b</sup>, Cedric J. Ginestra<sup>c</sup>, Yeshayahu Talmon<sup>b</sup>, Matteo Pasquali<sup>a,c,d,f</sup>, and Angel A. Martí<sup>\*,a,d,e,f</sup>

- a. Department of Chemistry, Rice University, Houston, Texas 77005, USA
- b. Department of Chemical Engineering and the Russell Berrie Nanotechnology Institute (RBNI), Technion Israel Institute of Technology, Haifa 3200003, Israel
- c. Department of Chemical and Biomolecular Engineering, Rice University, Houston, Texas 77005, USA
- d. Department of Materials Science and Nanoengineering, Rice University, Houston, Texas 77005, USA
- e. Department of Bioengineering, Rice University, Houston, Texas 77005, USA
- f. Smalley-Curl Institute for Nanoscale Science and Technology, Rice University, Houston, Texas 77005, USA
- † These authors contributed equally to this manuscript
- \* Corresponding author: amarti@rice.edu

### **Abstract**

Hexagonal boron nitride (hBN) is a structural analog of graphene, with unique mechanical, thermal, and optical properties that make it desirable for a variety of applications. Production of stable dispersions of well-exfoliated hBN nanosheets, particularly in a nontoxic and inexpensive way, is an important step in the production of hBN macromaterials on an industrial scale. Here we investigate the use of surfactants for exfoliating and dispersing hBN in aqueous solution. Dispersions in nine different surfactants and water were compared based on dispersion yield, quality, and stability. It was revealed that at low centrifugal force, large-molecular-weight nonionic surfactants disperse the most material. In contrast, when stronger centrifugation is applied, all surfactants produce similar dispersion yields, with dispersions in ionic surfactants containing significantly more exfoliated nanosheets and remaining stable over much longer periods of time. Finally, to demonstrate the scalability and effectiveness of these systems for making macroscopic materials, a dispersion of hBN in sodium dodecyl sulfate (SDS) was used to produce a transparent hBN film that can be deposited on glass and potentially used as an antibacterial or thermally resistant coating.

Keywords: hexagonal boron nitride, nanosheets, surfactants, exfoliation, aqueous dispersion, coating

### Introduction

Hexagonal boron nitride (hBN), also known as "white graphene", is a structural analog of graphene, composed of a honeycomb-like structure of sp²-hybridized, alternating boron and nitrogen atoms, as shown in Figure 1. hBN has a large Young's modulus (~1 TPa),¹,² that does not suffer from increasing BN layers stacking,³ excellent thermal conductivity (~360 W/mK),⁴ approaching that of copper, and impressive thermal stability, not experiencing oxidation in air until temperatures greater than 900°C.⁵ Additionally, hBN has a wide band-gap (~5.9 eV), making it an electrical insulator,⁵ and it is nearly transparent to visible (vis) light.⁶ These unique and enticing properties make hBN a strong contender for a wide variety of potential applications, including its use as thermal and mechanical reinforcements for composites,<sup>7-12</sup> in two-dimensional composites with graphene for electronics applications,<sup>5,13-16</sup> and as lubricants,<sup>17,18</sup> among others<sup>6,19-25</sup>. Intriguingly, the polarity of the B-N bond and the range of edge functional groups present in the material give hBN a different surface charge distribution compared to that of graphene, which could influence its dispersibility.

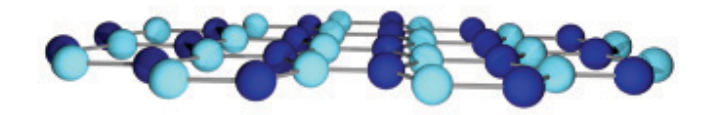
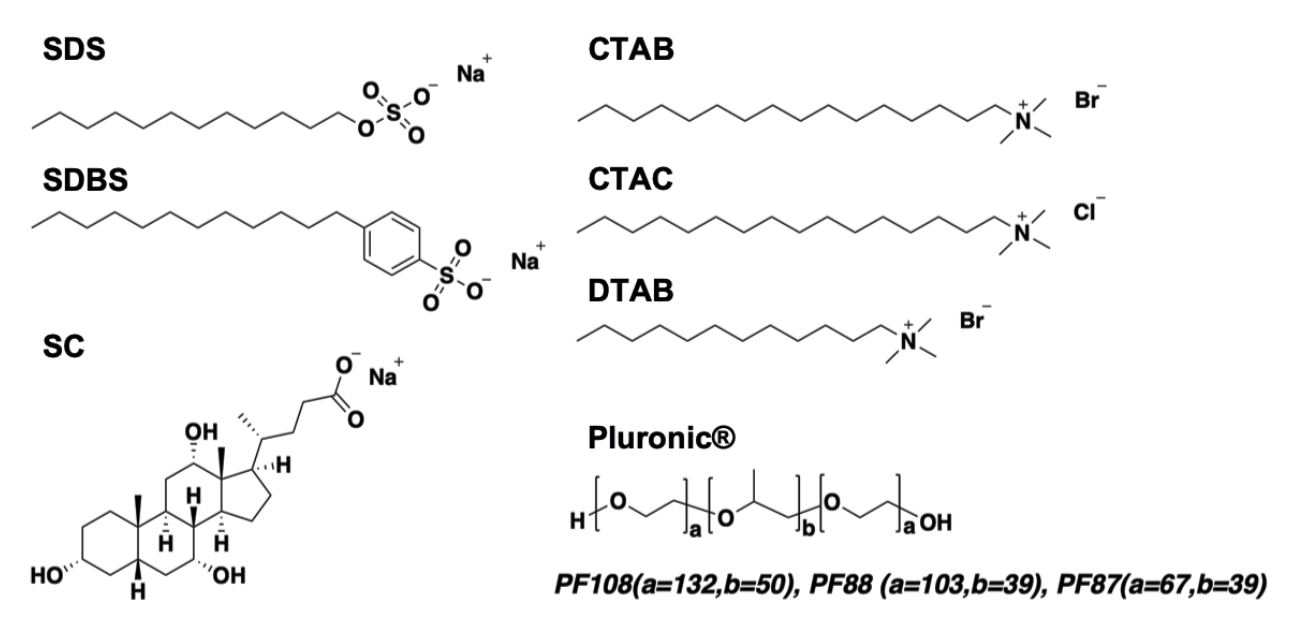


Figure 1. Schematic showing the honeycomb-like structure of hBN. These nanosheets extend laterally in two dimensions reaching micrometer sizes, with subnanometer thicknesses.

The top-down manufacturing of advanced materials made from this building block relies on the ability to produce stable dispersions of well-exfoliated hBN nanosheets (mono- or few-layer). The production of these dispersions on a large scale requires the exfoliation of the two-dimensional (2D) nanosheets from the three-dimensional (3D) bulk material. Some studies have explored exfoliation methods that can be applied to a variety of 2D materials, including graphene and transition metal dichalcogenides. Several groups have attempted to achieve hBN exfoliation in various ways, including the use of solvents, acids and bases, several functionalization, bifully biomolecules, several groups have attempted to achieve hBN exfoliation in various ways, including the use of solvents, acids and bases, several functionalization, bifully biomolecules, several groups have attempted to achieve hBN exfoliation in various ways, including the use of solvents, acids and bases, several groups have attempted to achieve hBN exfoliation, and bases, several groups have attempted to achieve hBN exfoliation, and surfactants, several groups, surfactants are advantageous for many industrial applications, as they have low toxicity, are inexpensive, and do not disrupt the sp² hybridization, and therefore the thermal and mechanical properties of hBN. Despite these advantages, very few surfactants have been tested for the dispersion of hBN. To the best of our knowledge, besides one report that utilized Pluronic F68, which did not report the dispersion yield, only anionic surfactants have been tested to date. Moreover, the wide variety of dispersion techniques applied prevents direct comparison from one report to the other. While significant progress has

been made, continued efforts are necessary to produce dispersions of well-exfoliated nanosheets at high concentrations, without significantly reducing the lateral dimensions from the bulk material. A systematic study of hBN dispersion in different types of surfactants is necessary to continue efforts toward optimizing their yield and exfoliation quality for industrial applications. Such studies have been performed on carbon nanotubes (CNTs),<sup>60</sup> boron nitride nanotubes (BNNTs),<sup>61</sup> and graphene,<sup>62</sup> and have been important references for others in the field.

In this work, we study the exfoliation and dispersion of hBN in aqueous solutions using nine surfactants commonly employed for the dispersion of nanoparticles (the surfactant structures are given in Figure 2). 28,60-62 Groups of anionic, cationic, and nonionic surfactants were used in order to study how the presence and type of ionic charges affect the dispersibility of hBN. As we suspect long periods of ball milling or ultrasonication, commonly used to produce these dispersions, <sup>28,51,52,54</sup> likely contribute to cutting of the lateral dimensions of the nanosheets, we stirred the mixtures to disperse the bulk material before applying a short period of bath sonication. Afterwards, the dispersions were subjected to two different centrifugation settings: one relatively low (100q), which produces high dispersion yield and provides a larger distinction between surfactants, and another relatively high (8,000a) to remove the majority of aggregates larger than few-layered nanosheets, optimizing dispersion quality and stability. The resulting dispersions were characterized by gravimetric, spectroscopic and microscopy experiments to assess the dispersion yield, exfoliation quality, and stability over time. The results of these experiments enabled us to elucidate how surfactant selection impacts the efficiency of the exfoliation and dispersion of hBN, which could then be used to make thermally resistant and antibacterial coatings.



**Figure 2.** The molecular structures of the nine surfactants used in this work. SDS = sodium dodecyl sulfate; SDBS = sodium dodecylbenzenesulfonate; SC = sodium cholate; CTAB = cetyltrimethylammonium bromide; CTAC = cetyltrimethylammonium chloride; DTAB = dodecyltrimethylammonium bromide; PF108 = Pluronic F108; PF88 = Pluronic F88; PF87 = Pluronic F87; Pluronic® = poly(ethylene oxide)-poly(propylene oxide)-poly(ethylene oxide) (PEO-PPO-PEO) triblock copolymer.

# **Experimental Section**

**Materials.** Hexagonal boron nitride was purchased from Sigma-Aldrich (powder, ~1  $\mu$ m, 98%); sodium dodecyl sulfate (SDS,  $\geq$  98.5%), sodium cholate (SC, SigmaUltra  $\geq$  99%) and sodium dodecylbenzenesulfonate (SDBS Technical grade) were purchased from Sigma-Aldrich; cetyltrimethylammonium bromide (CTAB 98%) was from Alfa Aesar; cetyltrimethylammonium chloride (CTAC 96%) was from BTC; dodecyltrimethylammonium bromide (DTAB 98%) was from TCI America; and Pluronic F108, F88, and F87 from BASF. All materials were used as received with no further purification.

Instrumentation. Thermogravimetric analysis (TGA) was performed with a Mettler Toledo TGA/DSC 3+ system. Samples were heated from 25°C to 1000°C at 10 °C/min. Atomic Force Microscopy (AFM) measurements were performed with a Nanoscope IIIa scanning probe microscope controller from Digital Instruments in tapping mode using silicon cantilevers. Cryogenic transmission electron microscopy (cryo-TEM) was performed with a Thermo Fisher (FEI) Talos 200C high-resolution TEM at an accelerating voltage of 200 kV. Specimens were maintained below -175 °C in the microscope using a Gatan 626 cryo-holder, and imaged in the low-dose imaging mode, to reduce electron-beam radiation-damage. Images were recorded digitally by a FEI Falcon III direct-imaging camera and TIA software, with the help of the "volta phase-plate" (FEI) to enhance image contrast. Absorbance measurements were acquired using a Shimadzu 2450 UV-Vis spectrophotometer. Samples prepared for absorbance measurements were centrifuged in glass inserts, as exposure to plastic can result in impurities that also absorbs in the UV. ζ potential measurements were obtained using a Malvern Zen 3600 Zetasizer with the dispersions injected into folded capillary cells. All measurements were conducted at 25°C and at the natural pH of the surfactant solution. Scanning electron microscopy (SEM) images of the prepared film were performed with a FEI Helios NanoLab 660 SEM. All images were taken without coating with a conductive layer. Charging was reduced by imaging at 1 kV, 50 pA, and at a close working distance of ~4 mm. X-ray photoelectron spectroscopy (XPS) measurements were performed using a Phi Quantera scanning X-ray microprobe. Survey scans were done at 140 eV, and 26 eV was used for high-resolution analysis.

**Preparation of Dispersions.** Surfactant concentration, stir time, and sonication time were roughly optimized in sodium cholate (SC, Table S1), but were kept the same for all surfactants for direct comparison. Approximately 20 mg hBN were added to a vial outfitted with a stir bar followed by 1 wt % surfactant solution for an initial concentration of 2 mg/mL. The solution was stirred for 1 h, bath-ultrasonicated for 20 min (Cole-Parmer 8891, 42 kHz), and then centrifuged at either 100*q* or 8000*q* for 30 min.

Determination of Dispersion Yield. For samples prepared by the 100g centrifugation method, the supernatant was filtered through a poly(tetrafluoroethylene) (PTFE) membrane (ADVANTEC, hydrophilic, 0.2µm pore size) twice and washed with plenty of water and isopropyl alcohol (IPA) to remove the surfactant. The filter was dried for 1 h at 110°C and the final mass of hBN recorded. This was divided by the initial mass of hBN and multiplied by 100% to get the dispersion yield.

For samples prepared by the 8,000g centrifugation method, the supernatant was collected in a separate vial for other measurements and the pellet was redispersed in water. The redispersed pellet was then filtered through the PTFE membrane filter and washed with water and IPA to remove the surfactant. The filter was dried for 1 hour at 110°C, and the final mass of

hBN was recorded. This was subtracted from the initial mass of hBN, to get the amount of hBN that was left in the supernatant, and then divided by the initial mass of hBN and multiplied by 100% to get the dispersion yield.

**Preparation of Control Sample.** Approximately 20 mg hBN were added to a vial with 10 mL of 1 wt % surfactant. This solution was sonicated for 20 min, then filtered through a PTFE membrane, washed with water and IPA to remove surfactant, and its final dry mass was recorded. As no centrifugation or transfer steps were undertaken, the final mass of hBN should be equal to the initial amount added. The final solid was analyzed by TGA to ensure all of the surfactant was removed during the washing process.

**Testing Dispersion Stability.** Dispersions were prepared as detailed above in water, SDS, CTAC, Pluronic F88, and Pluronic F87, and the supernatants were collected. These surfactants were chosen as their absorbance does not overlap too significantly with that of hBN. For the 8,000*g* centrifugation method, UV-vis absorbance measurements were taken on Days 0, 1, 3, 5, 7, 14, 21, 24, and 90. The absorbance was measured from 190 to 500 nm with 1 nm wavelength resolution. The absorbance of free surfactant solution was subtracted, and the resulting absorbance at 205 nm was recorded and tracked over time. After the initial measurement, the samples were diluted with a surfactant solution, adjusting all samples to have the same initial hBN concentration.

For the 100g centrifugation method, UV-vis absorbance measurements were only taken on days 0 and 1, as a significant amount of material had crashed out of solution after 24 h. For each absorbance measurement, 0.1 mL of the concentrated sample was added to 3 mL of DI water. The absorbance of free surfactant solution diluted by the same amount was subtracted, and the resulting absorbance at 205 nm was recorded for each time point.

**Preparation of AFM Samples.** The supernatant from each hBN dispersion was collected for imaging. AFM samples were prepared by depositing the hBN dispersion on a freshly cleaved mica surface (primed with MgCl<sub>2</sub>). The surface was heated to ~120°C using a hot plate, and the dispersion was applied through a spray bottle in order to deposit a fine mist that could quickly dry. For surfactant samples, excess surfactant was removed by dipping the mica into water (ionic surfactants) or methanol (Pluronic surfactants), and drying with air. This process was repeated twice before further washing with isopropanol (ionic surfactants) or methanol (Pluronic surfactants). All samples were left to dry in the oven at 110°C for 1 hour.

**Determining hBN sheet thickness and lateral width.** AFM images were processed using Gwyddion software. Profiles through the middle of about 100 randomly selected nanosheets were drawn and used to obtain height and width measurements for each sheet. The results were plotted in a histogram for each surfactant used and fitted to a Gaussian curve using MATLAB.

**Preparation of Cryo-TEM Specimens.** Specimens were prepared in a controlled environment vitrification system (CEVS) at a temperature of 25 °C and 100% relative humidity to prevent water evaporation. A drop of about 3  $\mu$ L was applied onto a perforated carbon film supported on a 3 mm copper TEM grid. The drop was blotted with a filter paper to form a thin film (<300 nm) and was vitrified by plunging into liquid ethane at its freezing point.

**Preparing a Transparent hBN Coating.** Two hundred milligrams of hBN was dispersed in 100 mL of 1 wt % SDS according to our usual dispersion procedure of stirring, sonicating and centrifuging. The dispersed material was centrifuged at 1000g for 30 min to remove large aggregates and then filtered through an alumina membrane and washed with isopropanol. The

film produced on top of the filter was dried in an oven at 110°C overnight, and then floated on water. A transparent coating of hBN was deposited onto a glass slide or Al stubs for SEM imaging.

# **Results and Discussion**

The dispersions of hBN in aqueous solutions using nine different surfactants were analyzed based on dispersion yield, stability over time, and exfoliation quality (nanosheet thickness and lateral width). As detailed in the experimental section, for each dispersion, hBN was added to a 1 wt % solution of surfactant to make a 2 mg/mL initial concentration of hBN. The solution was stirred for 1 h, bath-sonicated for 20 min (42 kHz), and then centrifuged for 30 min at either 100g or 8000g. The mass of hBN that remained dispersed in the supernatant after centrifugation was determined by filtration and weighing. The stirring step was added in an attempt to reduce the long sonication times commonly used for these dispersions and to preserve the lateral dimensions of the nanosheets.<sup>28,52</sup> The very low centrifugal force (100g) maximized hBN dispersion yield and provided a greater distinction between the surfactants, while the larger centrifugal force (8000g) resulted in improved dispersion quality and stability. Control experiments were performed for each surfactant, with no centrifugation step, to ensure all material was recovered and that the surfactant was completely removed during the washing steps, as confirmed by TGA (Figure S1).

Figure 3 presents the dispersion yields obtained for both the 100q and 8000q centrifugation preparations for all nine surfactants and water. The hBN dispersion yields for the 100g centrifugation preparation ranged between ca. 3 and 16%. Pluronic surfactants best dispersed hBN under these conditions, with yields ranging between ca. 8 and 16%. Within this group, Pluronic F88 (molecular weight (MW) ~11,400 g/mol, 80% hydrophilic) produced the largest yield of dispersed hBN (ca. 16%), compared to the larger PF108 (MW~14,600 g/mol, 80% hydrophilic) and the smaller PF87 (MW~7,700 g/mol, 70% hydrophilic), indicating there was no effect from the surfactant size in this case. After the nonionic surfactants, the three anionic surfactants (SDS, SDBS, and SC) and DTAB (cationic) all disperse approximately the same amount of material (ca. 5%), while CTAB and CTAC (also cationic) disperse the least (ca. 3%), regardless of ion size or pH. These results are similar to the results previously reported for graphene. 62 For the ionic surfactants, we observed that in this case dispersion might be related to surfactant size. SDS, SDBS, and DTAB all have a 12-carbon aliphatic tail, while CTAC and CTAB have a 16-carbon hydrophobic tail. Likely, the shorter aliphatic chains interact more easily with exfoliated hBN nanosheets and stabilize them. Smith and coworkers saw a similar result when comparing CTAB and TTAB (tetradecyltrimethylammonium bromide) in the dispersion of graphene.<sup>62</sup> Moreover, it is expected that the steroid structure of SC and the benzene ring in SDBS promote these interactions even further, which would compensate for their larger size and it is likely why these ionic surfactants have been so commonly utilized for making dispersions of hBN and other 2D materials, <sup>28,52,62,64,65</sup> however, no marked differences were observed when compared with SDS.

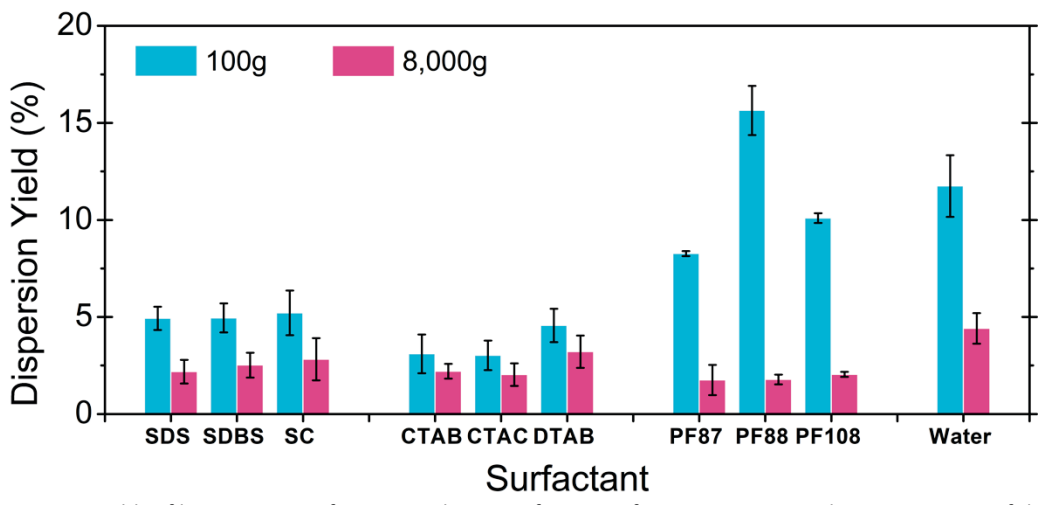


**Figure 3.** Dispersion yields of hBN in nine surfactants and water, after centrifugation at 100*g* and 8,000*g*. Images of the produced dispersions can be found in Figures S2 and S3.

When the dispersions are centrifuged at 8000q, the mass conversion results are similar for all of the surfactants (ca. 2-3% for all surfactants). Similar yields (20-25 µg/mL) were also obtained by Smith et al. for the dispersion of graphene with different ionic surfactants, with the exception of SDS and lithium dodecyl sulfate (LDS) that produce 10 µg/mL dispersions.<sup>62</sup> This could mean that surfactants do not have an important role in the exfoliation process; rather, they are important in stabilizing the nanosheets as soon as they become exfoliated. In addition, it should be noted that water, without the addition of surfactant, showed a larger dispersion yield than most of the surfactant solutions at both centrifugal forces. While this might sound counterintuitive when compared to other layered materials, such as graphene, the key is in the edge termination of hBN, which contains polar groups that make them somewhat hydrophilic. The top and bottom parts of an hBN crystal are formed of basal plane layers, which can be relatively hydrophobic. However, the sides have boron oxide and amine terminations, evidenced by XPS (Figure S4), which make the sides of the crystal hydrophilic.<sup>66</sup> Therefore, a large area of the surface of hBN (particularly when multiple layers are stacked) is hydrophilic enough for it to disperse in water. Wang and co-workers previously reported that surfactants can reduce the amount of hBN that is dispersed into solution, but they can improve the dispersion stability.<sup>53</sup> Therefore, we expect the quality of hBN dispersions in water alone to be poor in comparison to those prepared with surfactants, which will be evaluated by stability tests and imaging shown below. Hydrolysis of hBN by sonication in water has also been reported,44 however, we do not expect the short sonication time used here to be enough for this to occur to a significant extent.

In addition to a large dispersion yield, it would be beneficial for many applications to have dispersions that remain stable for extended periods of time. The best way to test this is with periodic UV-vis absorbance measurements, measuring the concentration of hBN and how it changes over time. Dispersions prepared in four of the surfactants and water were tracked by UV-vis for 24 days (Figure 4). The surfactants chosen were those that overlapped the least with hBN absorbance ( $\lambda_{max}$  = 205 nm), and could, therefore, have the surfactant absorbance subtracted as background. Dispersions were prepared as usual, by the 8000g centrifugation method, and then, the supernatant was collected and diluted with surfactant so all dispersions had the same initial hBN concentration. The diluted dispersions were left undisturbed. Samples

prepared by the 100g centrifugation method all experience  $\geq$  30% fallout within 24 h; thus long-term stability tests were not conducted.

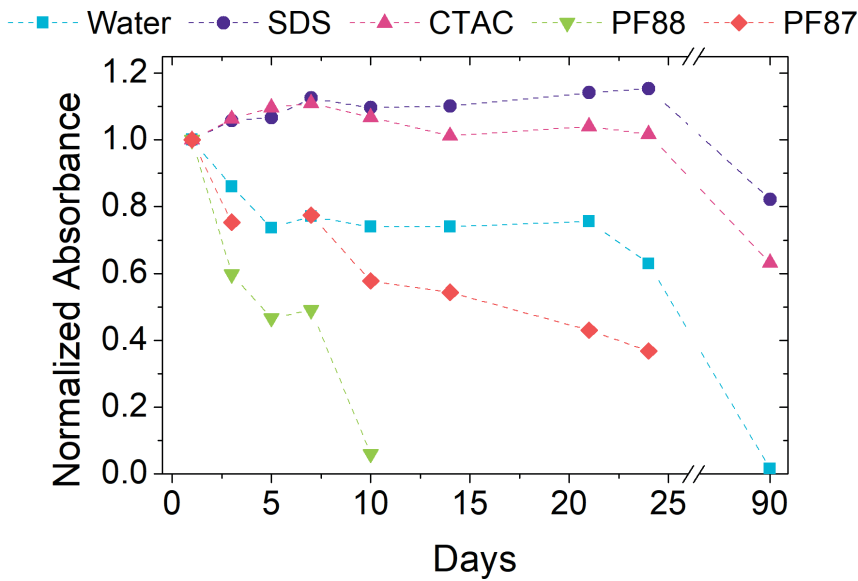


Figure 4. UV absorbance (at 205 nm) of hBN dispersions in surfactant solutions and water tracked over 24 days.

There were clear differences in the stability of the hBN dispersions for the surfactants tested. The ionic surfactant dispersions, SDS and CTAC, remained stable for the duration of the experiment. Though we could not test the other ionic surfactants, due to their large absorbance at 205 nm, we expect they would follow a similar trend, particularly after considering microscopy results, as shown below. By comparison, the nonionic surfactant dispersions were not as stable over time. The hBN concentration in PF88 fell below a detectable amount after day 10, and dispersions in PF87 also showed a considerable decrease in concentration over time (~63%). Water also showed a significant drop in concentration over time, with a ~37% decrease in absorbance over 24 days, a smaller drop than with the Pluronic surfactants, likely aided by the edge –OH and –NH groups present on the nanosheets.<sup>44</sup> It seems that without the electrostatic interactions provided by ionic surfactants, these dispersions (either in water by itself or with nonionic surfactants) are more prone to aggregating and crashing out of solution. The water, SDS, and CTAC samples were inspected again after 90 days. While the water dispersion had crashed out completely by that time, SDS and CTAC maintained 82 and 63% of their original hBN concentration, respectively, further confirming the stability of dispersions in ionic surfactants. In all, while dispersions prepared at low centrifugation show a larger dispersion yield, they are not stable over time. In contrast, dispersions prepared with higher centrifugal forces have a lower yield but are significantly more stable. In particular, the ones prepared with ionic surfactants show remarkable stability over time.

 $\zeta$  potential measurements were performed in an attempt to further elucidate the dispersion yield results, and to verify the stabilization mechanism. Measurements were taken of the dispersions in nine different surfactants and water. For all ionic dispersions, which are stabilized by electrostatic interactions, the  $|\zeta|$  is greater than the accepted value for colloidal stability (~25 mV), meaning restacking and aggregation of the hBN nanosheets should be minimal

(Figure 5).<sup>62</sup> The dispersion in water also has a  $|\zeta|$  slightly higher than 25 mV, indicating some electrostatic stabilization, likely from the hydrophilic groups on the sheets' edges. Finally, the  $|\zeta|$  for all dispersions in nonionic surfactants was less than 25 mV. This was not surprising, as the stabilization mechanism for these surfactants is steric rather than electrostatic in nature. In previous studies with boron nitride nanotubes and graphene, the  $|\zeta|$  of the dispersions in ionic surfactants trended with the concentration of material that was dispersed.<sup>61,62</sup> In this case, however, there is no apparent correlation. These results support our earlier suggestion that surfactants may not have an important role in the exfoliation process, and, therefore, do not dictate dispersion yield, but rather, are necessary to maintain the dispersion stability.

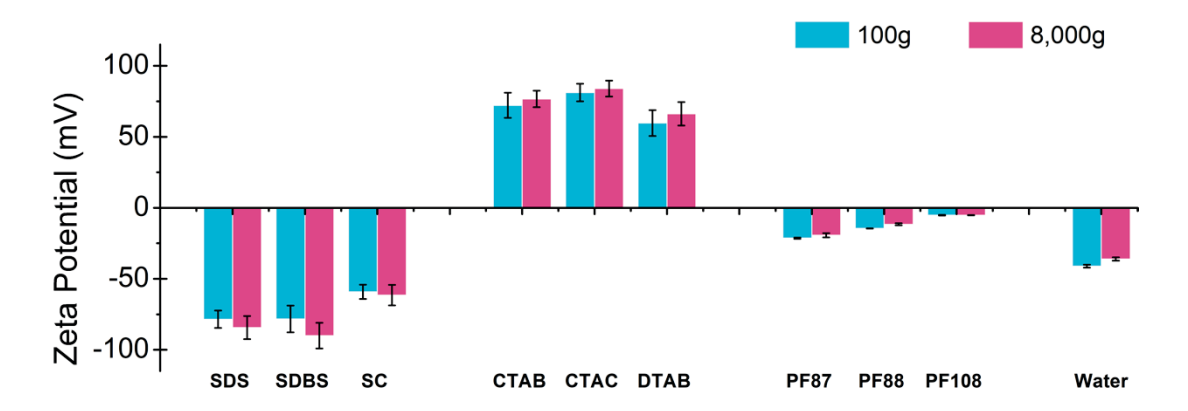
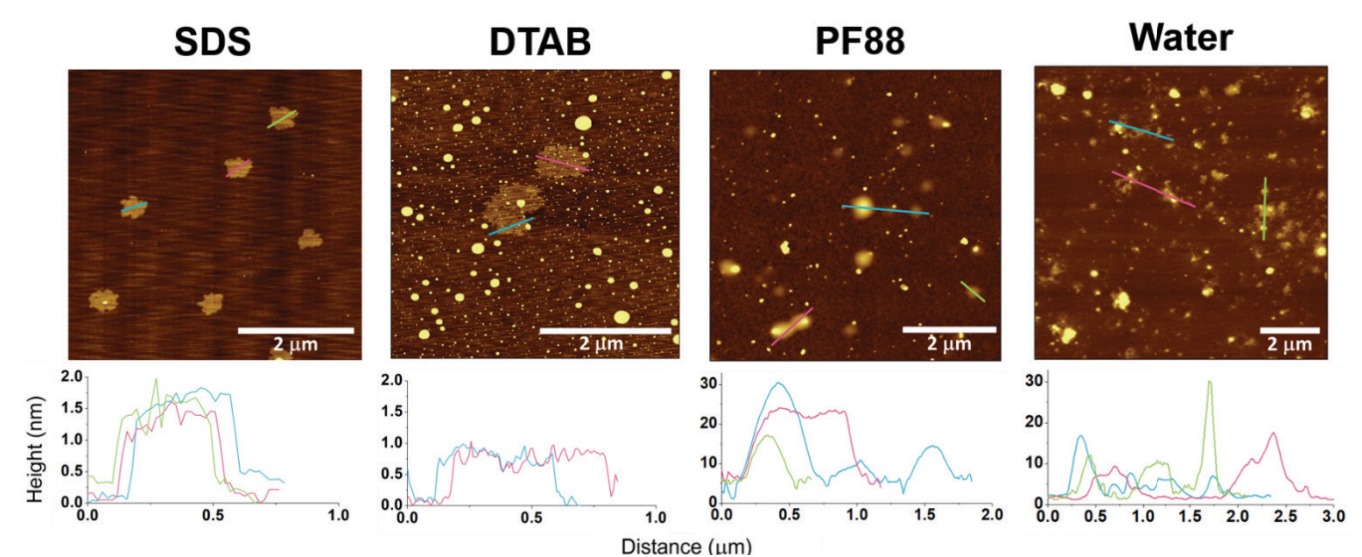


Figure 5. Zeta potential measured for hBN dispersions in the nine surfactants and water centrifuged at 100g and 8,000g.

Perhaps, the most important attribute of these dispersions is the quality of the dispersed material; i.e., the extent of exfoliation and sheet diameters. AFM imaging was utilized to determine the thickness and lateral length of the hBN in these surfactant dispersions (Figure 6 and Figure S5 and S6). After 100g centrifugation, AFM images show that all dispersions look similar, containing mostly large aggregated crystals up to about 250 nm in height, with very few exfoliated nanosheets present (Figure S5). Only dispersions in CTAB showed exfoliated nanosheets more frequently, while still having large aggregates within the sample. This aggregation correlates to their low stability over time, mentioned previously, and tendency to flocculate. Moreover, it can help explain why water and the nonionic surfactants could produce much greater dispersion yields than the ionic surfactants after the low centrifugation trials. The hBN aggregates (with hundreds of stacked sheets) have two very different surfaces; the top and bottom, which are relatively hydrophobic, and the outside edges, which are hydrophilic. In the case of well-exfoliated nanosheets, the hydrophobic tail of a surfactant interacts with the large hydrophobic surface of the sheet and project its polar group into the water interphase, therefore increasing the sheet's solubility. However, as these nanosheets stack together forming these aggregates, the relative ratio between the hydrophobic and hydrophilic surface areas decreases. In this case, the association of the surfactant to the, now much larger, hydrophilic surfaces results in a reduction of the hydrophilicity of the material, and reduces its dispersibility in water. For ionic surfactants, which rely on electrostatic interactions to maintain dispersion stability, this results in a low dispersion yield. On the contrary, nonionic surfactants utilize steric stabilization, with their large hydrophilic groups extending and swelling into the aqueous environment around

the nanosheet, giving more stabilization to the large stacked crystals.<sup>67</sup> Furthermore, without surfactant, the increased surface area of hydrophilic group due to stacked layers promotes the hBN crystal's affinity for water, producing a relatively large dispersion yield in water alone. Unfortunately, regardless of surfactant utilization, the large size of the particles makes the dispersions unstable and they severely flocculate within 24 hours.

On the contrary, in samples centrifuged at 8000*g*, considerably more exfoliated nanosheets could be located. Samples could be differentiated based on the surfactant used, showing primarily individual nanosheets in images of ionic surfactant dispersions and primarily aggregates in nonionic surfactants (with the exception of Pluronic F87) and water. Figure 6 shows representative images demonstrating this pattern, and images from all dispersions can be found in Figure S6. This pattern was further confirmed by cryo-TEM images of dispersions in SDS, DTAB, Pluronic F88, and water after 8000*g* centrifugation (Figure 7 and Figure S10). As seen by AFM, dispersions in SDS and DTAB reveal thin, exfoliated nanosheets, with unform, rather low contrast against the water, while dispersions in PF88 and water reveal large aggregates of material, showing much larger contrast, especially where particles overlap (arrows).



**Figure 6.** Representative AFM images and height profiles for a sampling of the surfactants and water at 8000*g* centrifugation. Bright yellow areas in surfactant samples are from excess surfactant that did not get removed (Figure S6, phase image).

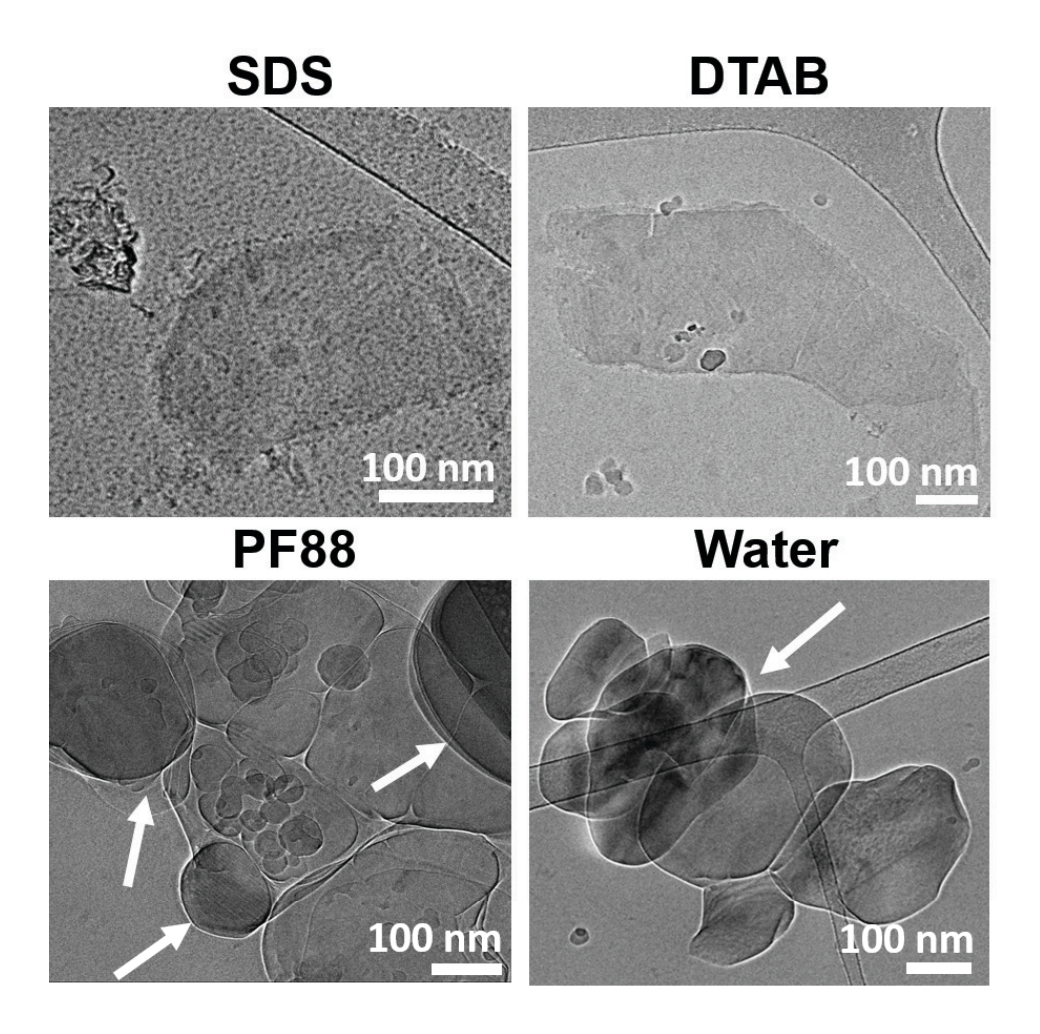


**Figure 7.** Cryo-TEM images of hBN dispersions in SDS, DTAB, Pluronic F88, all 1.0 wt %, and water. Note in SDS and DTAB thin, exfoliated nanosheets, with uniform, rather low contrast against the water, while in dispersions in PF88 and water, one sees large aggregates of material showing much larger contrast, especially where particles overlap (arrows). Black spots in the image are surfactant micelles.

To further analyze the quality of these dispersions after 8000g centrifugation, about a hundred randomly selected hBN nanosheets for each dispersion were measured and plotted in histograms to visualize trends in sheet thickness and lateral width for each surfactant and water (Figures S7-S9). The histograms were each fitted to a Gaussian distribution, and the mean ( $\mu$ ) was used to estimate the average thickness and lateral width of each dispersion. The results are summarized in Figure 8. First, when comparing the thickness of the resulting hBN nanosheets, two different types of dispersions were found. All the ionic surfactants and nonionic Pluronic F87 produced dispersions with more exfoliated hBN nanosheets, with average thicknesses ranging from 0.8 nm (DTAB) to 1.8 nm (SDS) (Figure S7). This nanosheet thickness is similar to other reports of effectively exfoliated hBN using surfactants,  $^{68}$  indicating sheets with individual or very few layers were achieved. On the contrary, Pluronic F88, Pluronic F108, and water still contained hBN crystals with average thicknesses of 12-16 nm (Figure S7 and S9).

This difference in sheet thickness can again be explained by each surfactant's different dispersion stability mechanism. As mentioned above, it appears unlikely that the surfactant plays a role in the exfoliation process but rather is necessary for dispersion stabilization, with sonication providing enough shear to exfoliate the hBN crystals into thin nanosheets. For ionic surfactants, the hydrophobic tail of the surfactant seems to adhere to the basal hBN plane, preventing stacking with other hBN nanosheets and stabilizing the dispersion by projecting their ionic group into the water interphase. In the case of the nonionic surfactants tested, the same is expected to happen, but as they have no ionic groups, they are not as efficient in stabilizing the dispersion and keeping the sheets from reaggregating. This is reflected by the thicker crystals observed for PF88 and PF108, which are similar to those observed in water. On the contrary, PF87 can stabilize thinner nanosheets and provide a longer stability time. This is thought to be due to its smaller size (MW ~7700 g/mol) and larger proportion of poly(propylene oxide) (PPO) groups (30% hydrophobic) compared to PF88 and PF108. Given the higher content of PPO groups, PF87 is expected to bind strongly to the surface of hBN, hiding from water both the PPO groups of the surfactant and the basal plane of hBN, and projecting the poly(ethylene oxide) (PEO) groups into the water interface. While PF87 produces good exfoliation of hBN, the stability tests show that the dispersions in ionic surfactants such as SDS and CTAC are even more stable over time. This indicates that repulsive electrostatic interactions produced by ionic surfactants are more efficient in stabilizing the dispersions than steric stabilization in Pluronic surfactants, while also producing the most exfoliated nanosheets.

The average lateral width for the hBN nanosheets in the dispersions ranged from 310 nm (SC) to 854 nm (PF108) (Figure S8 and S9). Generally, the nonionic and anionic surfactants produced dispersions of smaller nanosheets on average (~300 to 450 nm each) than the cationic surfactants (~500 to 800 nm), with the exception of PF108. Overall, when the goal is to obtain the thinnest, most exfoliated nanosheets with the largest lateral dimensions, the best quality dispersions were prepared with DTAB, with an average thickness of 0.8 nm and the second-largest average lateral width of 805 nm.

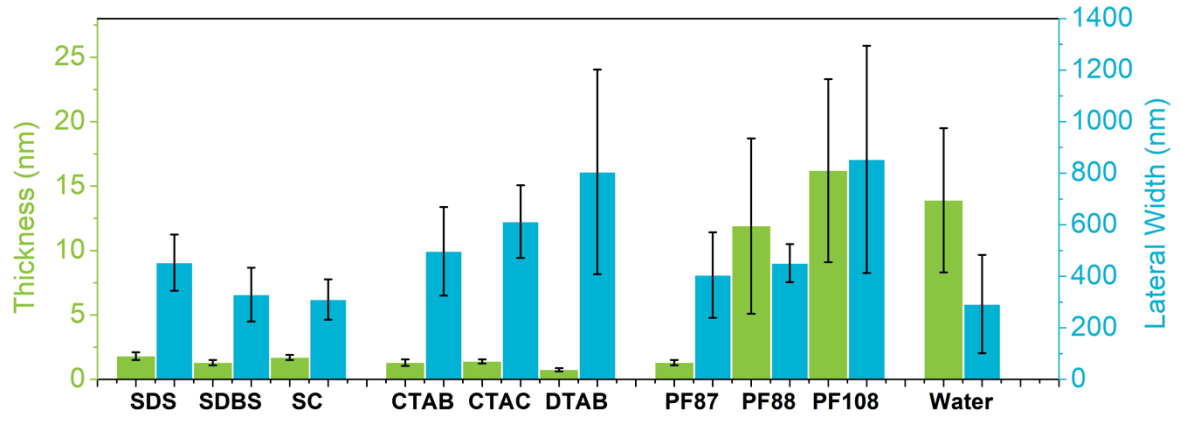
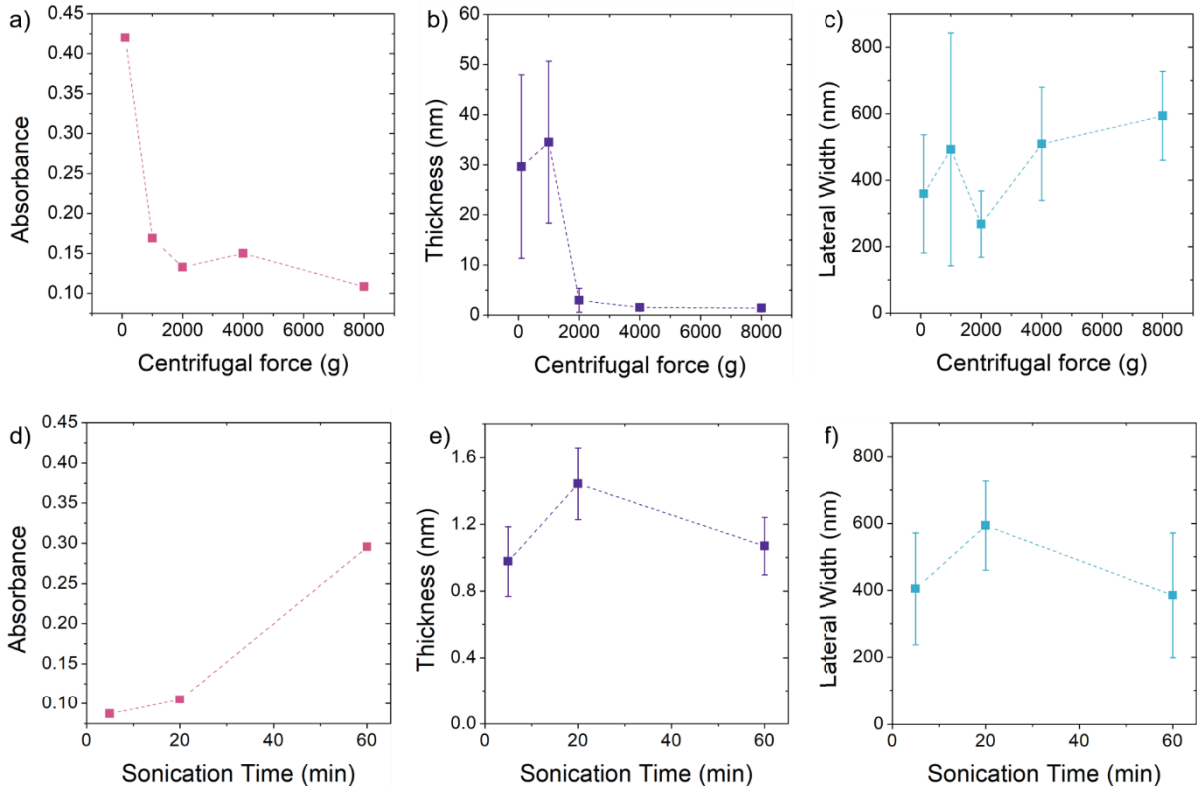


Figure 8. Average thickness and lateral width of 100 hBN nanosheets in the 10 dispersions after 8000g centrifugation.

Further studies were conducted to determine the impact of sonication time and centrifugal force on the yield and quality of the produced dispersions. Dispersions for these experiments were prepared using CTAC, as it produced the best quality nanosheets in dispersion (thinnest and largest), among the surfactants that we could be study by UV-vis. As mentioned previously, absorbance from DTAB, CTAB, SDBS, and SC overlaps considerably with that of hBN. First, to test the impact of centrifugation force, samples were prepared as usual but with centrifugal forces of 100q, 1000q, 2000q, 4000q, and 8000q. Then, to test the effect of increasing sonication time, samples were prepared as usual, but with varying sonication times of 5, 20, and 60 min. These samples were analyzed by UV-vis absorbance to determine the amount of hBN present in the dispersion and imaged by AFM to determine the relative quality of the produced dispersions, as determined by the thickness and lateral width of the sheets. Figure 9a-c shows the impact of centrifugal force on hBN concentration, thickness, and lateral width, respectively. As centrifugal force increases from 100q to 1000q the absorbance, and therefore concentration, of hBN is reduced almost three times but only experiences small reductions as the centrifugal force is further increased. This decrease in concentration also correlates with a decrease in average thickness, as aggregates are forced out of solution. The lateral width distribution of the nanosheets also decreases slightly as centrifugal force increases, but the overall impact is minimal. Figure 9d-f reveals the impact of increasing sonication time on the quantity and quality of dispersed hBN material. As sonication time is increased, the absorbance increases, as more material is able to exfoliate and get into solution. Changes in the thickness and lateral dimensions of the nanosheets are within error for all the sonication times tested. Overall, it appears that increasing the sonication time to 60 min increases the concentration of material in solution, with little impact on the lateral width and thickness of the sheets. Thus it seems that the ideal parameters for maximizing dispersion yield, while maintaining dispersion quality, are ~60 min sonication time paired with a centrifugal force between 2000g and 8000g. Much longer sonication times or increased sonication power, as utilized in previous studies,<sup>28,52</sup> are still expected to result in a dramatic reduction in lateral width.



**Figure 9.** Plots showing the impact of centrifugal force (a-c) and sonication time (d-f) on hBN sheet concentration, thickness, and lateral width. As centrifugal force increases, we see a decrease in absorbance (a) and thickness (b) with little impact on lateral dimensions (c). As sonication time increases, we see an increase in absorbance (d), and fairly insignificant changes in thickness (e), or lateral width (f).

Finally, to demonstrate the scalability and usefulness of these systems for making macroscopic materials, a dispersion prepared in SDS was used to produce a thin, transparent coating on glass (Figure 10a). Such hBN coatings have been proposed for bacterial growth suppression<sup>20,69</sup> or fire protection.<sup>70</sup> Since hBN is completely transparent to visible light, such coatings could be applied to imaging or detection systems without obscuring the signal. This was demonstrated by placing the coating over an image (Figure 10b). SEM imaging of the prepared film reveals a uniform layer of hBN nanosheets (Figure 10c,d). The thickness of these films was estimated using AFM to be ca. 400 nm.

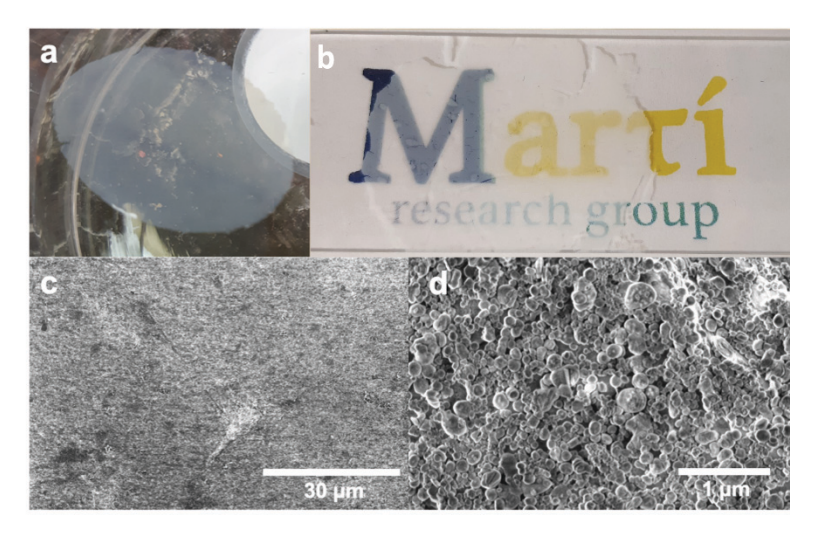


**Figure 10.** Transparent coating of hBN floating on water (a) and deposited on glass (b), showing the image is not obscured by the film. SEM images (c,d) of the film reveal a relatively uniform layer of hBN nanosheets.

# Conclusion

A systematic study of hBN dispersion in nine surfactants and water was conducted under two different dispersion preparation conditions. The dispersions were either centrifuged at a low centrifugal force (100g) to optimize the dispersion yield, and produce a greater distinction between surfactants, or at a higher force (8000q) to optimize the dispersion quality and stability. It was determined that after 100g centrifugation, nonionic surfactants, and particularly PF88 (MW ~11400 g/mol), dispersed the most material (ca. 16% yield). However, the quality of these dispersions was poor, primarily consisting of small stacked crystals of hBN rather than exfoliated nanosheets. After 8000q centrifugation, all of the surfactants had very similar dispersion yields (ca. 2-3%) and all dispersed less material than water alone; however, the quality and stability of the dispersions produced by ionic surfactants greatly surpassed those produced by nonionic surfactants or water. Additionally, dispersions in ionic surfactants, SDS and CTAC, could be monitored by UV-vis and were found to remain stable for at least 24 days, while those in nonionic surfactants and water experience significant fallout over time. Finally, a transparent coating of hBN on glass was prepared from a dispersion of hBN in an SDS aqueous solution, demonstrating the applicability of these systems to produce macroscopic materials. These films could be used in applications including antibacterial or thermally resistant coatings.

Through a combination of gravimetric, spectroscopic, and microscopy experiments, we determined that cationic surfactants, and more specifically DTAB, are the best choice for efficient exfoliation and dispersion of hBN. However, the similarity in results for all ionic surfactants reveals that the specific surfactant selection can be optimized based on the intended application, without fearing a major loss in dispersion yield or quality. Moreover, we found that our dispersion method, utilizing a combination of stirring, short sonication times, and high centrifugal forces, was ideal for preserving hBN sheet lateral dimensions while still obtaining dispersions of primarily thin, few-layered hBN nanosheets. Future work could aim to optimize these dispersion conditions further to increase dispersion yield without compromising quality or stability.

# Acknowledgements

A.A.M and M.P. acknowledge the National Science Foundation (CHE-1807737) and AFOSR (FA9550-18-1-0014) for financial support. Y.T.'s group work is supported by an AFOSR (FA9550-19-1-7045) grant. C.M.J. acknowledges the financial support from the CONACyT fellowship (Mexico, 710115). The cryo-TEM work was performed at the Technion Laboratory for Electron Microscopy of Soft Materials, support by the Technion Russell Berrie Nanotechnology Institute (RBNI). We also thank Cheol Park and Sang-Hyon Chu for helpful discussions, and Lyndsey Scammell (BNNT, LLC) for helpful discussions and assistance procuring material for this study.

# References

- (1) Chopra, N. G.; Zettl, A. Measurement of the Elastic Modulus of a Multi-Wall Boron Nitride Nanotube. *Solid State Commun.* **1998**, *105* (5), 297–300. https://doi.org/10.1016/S0038-1098(97)10125-9.
- (2) Falin, A.; Cai, Q.; Santos, E. J. G.; Scullion, D.; Qian, D.; Zhang, R.; Yang, Z.; Huang, S.; Watanabe, K.; Taniguchi, T.; Barnett, M. R.; Chen, Y.; Ruoff, R. S.; Li, L. H. Mechanical Properties of Atomically Thin Boron Nitride and the Role of Interlayer Interactions. *Nat. Commun.* **2017**, *8* (1), 1–9. https://doi.org/10.1038/ncomms15815.
- (3) Kim, S. M.; Hsu, A.; Park, M. H.; Chae, S. H.; Yun, S. J.; Lee, J. S.; Cho, D. H.; Fang, W.; Lee, C.; Palacios, T.; Dresselhaus, M.; Kim, K. K.; Lee, Y. H.; Kong, J. Synthesis of Large-Area Multilayer Hexagonal Boron Nitride for High Material Performance. *Nat. Commun.* **2015**, *6* (1), 1–11. https://doi.org/10.1038/ncomms9662.
- (4) Jo, I.; Pettes, M. T.; Kim, J.; Watanabe, K.; Taniguchi, T.; Yao, Z.; Shi, L. Thermal Conductivity and Phonon Transport in Suspended Few-Layer Hexagonal Boron Nitride. *Nano Lett.* **2013**, *13* (2), 550–554. https://doi.org/10.1021/nl304060g.
- (5) Wang, J.; Ma, F.; Sun, M. Graphene, Hexagonal Boron Nitride, and Their Heterostructures: Properties and Applications. *RSC Adv.* **2017**, *7* (27), 16801–16822. https://doi.org/10.1039/c7ra00260b.
- (6) Lei, W.; Mochalin, V. N.; Liu, D.; Qin, S.; Gogotsi, Y.; Chen, Y. Boron Nitride Colloidal Solutions, Ultralight Aerogels and Freestanding Membranes through One-Step Exfoliation and Functionalization. *Nat. Commun.* **2015**, *6* (1), 1–8. https://doi.org/10.1038/ncomms9849.
- (7) Zhi, C.; Bando, Y.; Tang, C.; Kuwahara, H.; Golberg, D. Large-Scale Fabrication of Boron Nitride Nanosheets and Their Utilization in Polymeric Composites with Improved Thermal and Mechanical Properties. Adv. Mater. 2009, 21 (28), 2889–2893. https://doi.org/10.1002/adma.200900323.
- (8) Sato, K.; Horibe, H.; Shirai, T.; Hotta, Y.; Nakano, H.; Nagai, H.; Mitsuishi, K.; Watari, K. Thermally Conductive Composite Films of Hexagonal Boron Nitride and Polyimide with Affinity-Enhanced Interfaces. *J. Mater. Chem.* **2010**, *20* (14), 2749–2752. https://doi.org/10.1039/b924997d.
- (9) Owuor, P. S.; Park, O. K.; Woellner, C. F.; Jalilov, A. S.; Susarla, S.; Joyner, J.; Ozden, S.; Duy, L.; Salvatierra, R. V.; Vajtai, R.; Tour, J. M.; Lou, J.; Galvão, D. S.; Tiwary, C. S.; Ajayan, P. M. Lightweight Hexagonal Boron Nitride Foam for CO2 Absorption. *ACS Nano* **2017**, *11* (9), 8944–8952. https://doi.org/10.1021/acsnano.7b03291.

- (10) Guerra, V.; Wan, C.; McNally, T. Thermal Conductivity of 2D Nano-Structured Boron Nitride (BN) and Its Composites with Polymers. *Prog. Mater. Sci.* **2019**, *100*, 170–186. https://doi.org/10.1016/j.pmatsci.2018.10.002.
- (11) Wang, Z.; Wen, Y.; Zhao, S.; Zhang, W.; Ji, Y.; Zhang, S.; Li, J. Soy Protein as a Sustainable Surfactant to Functionalize Boron Nitride Nanosheets and Its Application for Preparing Thermally Conductive Biobased Composites. *Ind. Crops Prod.* **2019**, *137*, 239–247. https://doi.org/10.1016/j.indcrop.2019.04.054.
- (12) Yang, W.; Yuen, A. C. Y.; Ping, P.; Wei, R. C.; Hua, L.; Zhu, Z.; Li, A.; Zhu, S. E.; Wang, L. L.; Liang, J.; Chen, T. B. Y.; Yu, B.; Si, J. Y.; Lu, H. D.; Chan, Q. N.; Yeoh, G. H. Pectin-Assisted Dispersion of Exfoliated Boron Nitride Nanosheets for Assembled Bio-Composite Aerogels. *Compos. Part A Appl. Sci. Manuf.* **2019**, *119*, 196–205. https://doi.org/10.1016/j.compositesa.2019.02.003.
- (13) Dean, C. R.; Young, A. F.; Meric, I.; Lee, C.; Wang, L.; Sorgenfrei, S.; Watanabe, K.; Taniguchi, T.; Kim, P.; Shepard, K. L.; Hone, J. Boron Nitride Substrates for High-Quality Graphene Electronics. *Nat. Nanotechnol.* **2010**, *5*, 722–726. https://doi.org/nnano.2010.172.
- (14) Lee, K. H.; Shin, H. J.; Lee, J.; Lee, I. Y.; Kim, G. H.; Choi, J. Y.; Kim, S. W. Large-Scale Synthesis of High-Quality Hexagonal Boron Nitride Nanosheets for Large-Area Graphene Electronics. *Nano Lett.* **2012**, *12* (2), 714–718. https://doi.org/10.1021/nl203635v.
- (15) Withers, F.; Del Pozo-Zamudio, O.; Schwarz, S.; Dufferwiel, S.; Walker, P. M.; Godde, T.; Rooney, A. P.; Gholinia, A.; Woods, C. R.; Blake, P.; Haigh, S. J.; Watanabe, K.; Taniguchi, T.; Aleiner, I. L.; Geim, A. K.; Fal'Ko, V. I.; Tartakovskii, A. I.; Novoselov, K. S. WSe2 Light-Emitting Tunneling Transistors with Enhanced Brightness at Room Temperature. *Nano Lett.* 2015, 15 (12), 8223–8228. https://doi.org/10.1021/acs.nanolett.5b03740.
- (16) Li, X.; Lin, S.; Lin, X.; Xu, Z.; Wang, P.; Zhang, S.; Zhong, H.; Xu, W.; Wu, Z.; Fang, W. Graphene/h-BN/GaAs Sandwich Diode as Solar Cell and Photodetector. *Opt. Express* **2016**, *24* (1), 134. https://doi.org/10.1364/oe.24.000134.
- (17) Bai, Y.; Zhang, J.; Wang, Y.; Cao, Z.; An, L.; Zhang, B.; Yu, Y.; Zhang, J.; Wang, C. Ball Milling of Hexagonal Boron Nitride Microflakes in Ammonia Fluoride Solution Gives Fluorinated Nanosheets That Serve as Effective Water-Dispersible Lubricant Additives. *ACS Appl. Nano Mater.* **2019**, *2* (5), 3187–3195. https://doi.org/10.1021/acsanm.9b00502.
- (18) Ma, Z. S.; Ding, H. L.; Liu, Z.; Cheng, Z. L. Preparation and Tribological Properties of Hydrothermally Exfoliated Ultrathin Hexagonal Boron Nitride Nanosheets (BNNSs) in Mixed NaOH/KOH Solution. *J. Alloys Compd.* **2019**, *784*, 807–815. https://doi.org/10.1016/j.jallcom.2019.01.108.
- (19) Li, L. H.; Xing, T.; Chen, Y.; Jones, R. Boron Nitride Nanosheets for Metal Protection. *Adv. Mater. Interfaces* **2014**, *1* (8), 1300132. https://doi.org/10.1002/admi.201300132.
- (20) Parra, C.; Montero-Silva, F.; Henríquez, R.; Flores, M.; Garín, C.; Ramírez, C.; Moreno, M.; Correa, J.; Seeger, M.; Häberle, P. Suppressing Bacterial Interaction with Copper Surfaces through Graphene and Hexagonal-Boron Nitride Coatings. *ACS Appl. Mater. Interfaces* **2015**, *7* (12), 6430–6437. https://doi.org/10.1021/acsami.5b01248.
- (21) Li, L. H.; Chen, Y. Atomically Thin Boron Nitride: Unique Properties and Applications. *Adv. Funct. Mater.* **2016**, *26* (16), 2594–2608. https://doi.org/10.1002/adfm.201504606.
- (22) Kim, N. Y.; Leem, Y. C.; Hong, S. H.; Park, J. H.; Yim, S. Y. Ultrasensitive and Stable

- Plasmonic Surface-Enhanced Raman Scattering Substrates Covered with Atomically Thin Monolayers: Effect of the Insulating Property. *ACS Appl. Mater. Interfaces* **2019**. https://doi.org/10.1021/acsami.8b17847.
- (23) Qiu, X.; Li, Z.; Li, X.; Yu, L.; Zhang, Z. Construction and Flame-retardant Performance of Layer-by-layer Assembled Hexagonal Boron Nitride Coatings on Flexible Polyurethane Foams. *J. Appl. Polym. Sci.* **2019**, *136* (29), 47839. https://doi.org/10.1002/app.47839.
- (24) Moraes, A. C. M.; Hyun, W. J.; Seo, J. T.; Downing, J. R.; Lim, J.; Hersam, M. C. Ion-Conductive, Viscosity-Tunable Hexagonal Boron Nitride Nanosheet Inks. *Adv. Funct. Mater.* **2019**, *29* (39), 1902245. https://doi.org/10.1002/adfm.201902245.
- (25) Khan, A. F.; Brownson, D. A. C.; Foster, C. W.; Smith, G. C.; Banks, C. E. Surfactant Exfoliated 2D Hexagonal Boron Nitride (2D-HBN) Explored as a Potential Electrochemical Sensor for Dopamine: Surfactants Significantly Influence Sensor Capabilities. *Analyst* **2017**, *142* (10), 1756–1764. https://doi.org/10.1039/c7an00323d.
- (26) Coleman, J. N.; Lotya, M.; O'Neill, A.; Bergin, S. D.; King, P. J.; Khan, U.; Young, K.; Gaucher, A.; De, S.; Smith, R. J.; Shvets, I. V.; Arora, S. K.; Stanton, G.; Kim, H. Y.; Lee, K.; Kim, G. T.; Duesberg, G. S.; Hallam, T.; Boland, J. J.; Wang, J. J.; Donegan, J. F.; Grunlan, J. C.; Moriarty, G.; Shmeliov, A.; Nicholls, R. J.; Perkins, J. M.; Grieveson, E. M.; Theuwissen, K.; McComb, D. W.; Nellist, P. D.; Nicolosi, V. Two-Dimensional Nanosheets Produced by Liquid Exfoliation of Layered Materials. *Science* (80-. ). 2011, 331 (6017), 568–571. https://doi.org/10.1126/science.1194975.
- (27) Shen, J.; Wu, J.; Wang, M.; Dong, P.; Xu, J.; Li, X.; Zhang, X.; Yuan, J.; Wang, X.; Ye, M.; Vajtai, R.; Lou, J.; Ajayan, P. M. Surface Tension Components Based Selection of Cosolvents for Efficient Liquid Phase Exfoliation of 2D Materials. *Small* **2016**, *12* (20), 2741–2749. https://doi.org/10.1002/smll.201503834.
- (28) Smith, R. J.; King, P. J.; Lotya, M.; Wirtz, C.; Khan, U.; De, S.; O'Neill, A.; Duesberg, G. S.; Grunlan, J. C.; Moriarty, G.; Chen, J.; Wang, J.; Minett, A. I.; Nicolosi, V.; Coleman, J. N. Large-Scale Exfoliation of Inorganic Layered Compounds in Aqueous Surfactant Solutions. *Adv. Mater.* **2011**, *23* (34), 3944–3948. https://doi.org/10.1002/adma.201102584.
- (29) Yola, M. L.; Atar, N. Simultaneous Determination of β-Agonists on Hexagonal Boron Nitride Nanosheets/Multi-Walled Carbon Nanotubes Nanocomposite Modified Glassy Carbon Electrode. *Mater. Sci. Eng. C* **2019**, *96*, 669–676. https://doi.org/10.1016/j.msec.2018.12.004.
- (30) Shang, J.; Xue, F.; Fan, C.; Ding, E. Preparation of Few Layers Hexagonal Boron Nitride Nanosheets via High-Pressure Homogenization. *Mater. Lett.* **2016**, *181*, 144–147. https://doi.org/10.1016/j.matlet.2016.05.154.
- (31) Zhou, K.-G.; Mao, N.-N.; Wang, H.-X.; Peng, Y.; Zhang, H.-L. A Mixed-Solvent Strategy for Efficient Exfoliation of Inorganic Graphene Analogues. *Angew. Chemie Int. Ed.* **2011**, *50* (46), 10839–10842. https://doi.org/10.1002/anie.201105364.
- (32) Warner, J. H.; Rümmeli, M. H.; Bachmatiuk, A.; Büchner, B. Atomic Resolution Imaging and Topography of Boron Nitride Sheets Produced by Chemical Exfoliation. *ACS Nano* **2010**, *4* (3), 1299–1304. https://doi.org/10.1021/nn901648q.
- (33) Marsh, K. L.; Souliman, M.; Kaner, R. B. Co-Solvent Exfoliation and Suspension of Hexagonal Boron Nitride. *Chem. Commun.* **2015**, *51* (1), 187–190. https://doi.org/10.1039/c4cc07324j.

- (34) Kovtyukhova, N. I.; Perea-López, N.; Terrones, M.; Mallouk, T. E. Atomically Thin Layers of Graphene and Hexagonal Boron Nitride Made by Solvent Exfoliation of Their Phosphoric Acid Intercalation Compounds. *ACS Nano* **2017**, *11* (7), 6746–6754. https://doi.org/10.1021/acsnano.7b01311.
- (35) Jasuja, K.; Ayinde, K.; Wilson, C. L.; Behura, S. K.; Ikenbbery, M. A.; Moore, D.; Hohn, K.; Berry, V. Introduction of Protonated Sites on Exfoliated, Large-Area Sheets of Hexagonal Boron Nitride. *ACS Nano* **2018**, *12* (10), 9931–9939. https://doi.org/10.1021/acsnano.8b03651.
- (36) Zhao, H.-R.; Ding, J.-H.; Shao, Z.-Z.; Xu, B.-Y.; Zhou, Q.-B.; Yu, H.-B. High-Quality Boron Nitride Nanosheets and Their Bioinspired Thermally Conductive Papers. *ACS Appl. Mater. Interfaces* **2019**, *11* (40), 37247–37255. https://doi.org/10.1021/acsami.9b11180.
- (37) Du, M.; Wu, Y.; Hao, X. A Facile Chemical Exfoliation Method to Obtain Large Size Boron Nitride Nanosheets. *CrystEngComm* **2013**, *15* (9), 1782–1786. https://doi.org/10.1039/c2ce26446c.
- (38) Jin, W.; Zhang, W.; Gao, Y.; Liang, G.; Gu, A.; Yuan, L. Surface Functionalization of Hexagonal Boron Nitride and Its Effect on the Structure and Performance of Composites. *Appl. Surf. Sci.* **2013**, *270*, 561–571. https://doi.org/10.1016/j.apsusc.2013.01.086.
- (39) de los Reyes, C. A.; Hernández, K.; Martínez-Jiménez, C.; Walz Mitra, K. L.; Ginestra, C.; Smith McWilliams, A. D.; Pasquali, M.; Martí, A. A. Tunable Alkylation of White Graphene (Hexagonal Boron Nitride) Using Reductive Conditions. *J. Phys. Chem. C* **2019**, *123* (32), 19725–19733. https://doi.org/10.1021/acs.jpcc.9b05416.
- (40) Sainsbury, T.; Satti, A.; May, P.; O'Neill, A.; Nicolosi, V.; Gun'Ko, Y. K.; Coleman, J. N. Covalently Functionalized Hexagonal Boron Nitride Nanosheets by Nitrene Addition. *Chem. A Eur. J.* **2012**, *18* (35), 10808–10812. https://doi.org/10.1002/chem.201201734.
- (41) ul Ahmad, A.; Liang, H.; Abbas, Q.; Ali, S.; Iqbal, M.; Farid, A.; Abbas, A.; Farooq, Z. A Novel Mechano-Chemical Synthesis Route for Fluorination of Hexagonal Boron Nitride Nanosheets. *Ceram. Int.* **2019**, *45* (15), 19173–19181. https://doi.org/10.1016/j.ceramint.2019.06.164.
- (42) Jin, H.; Li, Y.; Li, X.; Shi, Z.; Xia, H.; Xu, Z.; Qiao, G. Functionalization of Hexagonal Boron Nitride in Large Scale by a Low-Temperature Oxidation Route. *Mater. Lett.* **2016**, *175*, 244–247. https://doi.org/10.1016/j.matlet.2016.04.008.
- (43) Cao, C.; Xue, Y.; Liu, Z.; Zhou, Z.; Ji, J.; Song, Q.; Hu, Q.; Fang, Y.; Tang, C. Scalable Exfoliation and Gradable Separation of Boric-Acid-Functionalized Boron Nitride Nanosheets. *2D Mater.* **2019**, *6* (3), 035014. https://doi.org/10.1088/2053-1583/ab0eb4.
- (44) Lin, Y.; Williams, T. V.; Xu, T. B.; Cao, W.; Elsayed-Ali, H. E.; Connell, J. W. Aqueous Dispersions of Few-Layered and Monolayered Hexagonal Boron Nitride Nanosheets from Sonication-Assisted Hydrolysis: Critical Role of Water. *J. Phys. Chem. C* **2011**, *115* (6), 2679–2685. https://doi.org/10.1021/jp110985w.
- (45) Deshmukh, A. R.; Jeong, J. W.; Lee, S. J.; Park, G. U.; Kim, B. S. Ultrasound-Assisted Facile Green Synthesis of Hexagonal Boron Nitride Nanosheets and Their Applications. *ACS Sustain. Chem. Eng.* **2019**, *7* (20), 17114–17125. https://doi.org/10.1021/acssuschemeng.9b03387.
- (46) Ge, X.; Liang, W. J.; Ge, J. F.; Chen, X. J.; Ji, J. Y.; Pang, X. Y.; He, M.; Feng, X. M. Hexagonal Boron Nitride/Microfibril Cellulose/ Poly(Vinyl Alcohol) Ternary Composite Film with

- Thermal Conductivity and Flexibility. *Materials (Basel).* **2018**, *12* (1), 104. https://doi.org/10.3390/ma12010104.
- (47) Song, W. L.; Wang, P.; Cao, L.; Anderson, A.; Meziani, M. J.; Farr, A. J.; Sun, Y. P. Polymer/Boron Nitride Nanocomposite Materials for Superior Thermal Transport Performance. *Angew. Chemie Int. Ed.* **2012**, *51* (26), 6498–6501. https://doi.org/10.1002/anie.201201689.
- (48) Lin, Y.; Williams, T. V.; Connell, J. W. Soluble, Exfoliated Hexagonal Boron Nitride Nanosheets. *J. Phys. Chem. Lett.* **2010**, *1* (1), 277–283. https://doi.org/10.1021/jz9002108.
- (49) Han, W. Q.; Wu, L.; Zhu, Y.; Watanabe, K.; Taniguchi, T. Structure of Chemically Derived Mono- and Few-Atomic-Layer Boron Nitride Sheets. *Appl. Phys. Lett.* **2008**, *93* (22), 223103. https://doi.org/10.1063/1.3041639.
- (50) Muhabie, A. A.; Cheng, C. C.; Huang, J. J.; Liao, Z. S.; Huang, S. Y.; Chiu, C. W.; Lee, D. J. Non-Covalently Functionalized Boron Nitride Mediated by a Highly Self-Assembled Supramolecular Polymer. *Chem. Mater.* 2017, 29 (19), 8513–8520. https://doi.org/10.1021/acs.chemmater.7b03426.
- (51) Zhu, J.; Kang, J.; Kang, J.; Jariwala, D.; Wood, J. D.; Seo, J. W. T.; Chen, K. S.; Marks, T. J.; Hersam, M. C. Solution-Processed Dielectrics Based on Thickness-Sorted Two-Dimensional Hexagonal Boron Nitride Nanosheets. *Nano Lett.* **2015**, *15* (10), 7029–7036. https://doi.org/10.1021/acs.nanolett.5b03075.
- (52) Chae, A.; Park, S. J.; Min, B.; In, I. Enhanced Dispersion of Boron Nitride Nanosheets in Aqueous Media by Using Bile Acid-Based Surfactants. *Mater. Res. Express* **2018**, *5* (1), 15036. https://doi.org/10.1088/2053-1591/aaa434.
- (53) Wang, W.; Chen, S. J.; Basquiroto De Souza, F.; Wu, B.; Duan, W. H. Exfoliation and Dispersion of Boron Nitride Nanosheets to Enhance Ordinary Portland Cement Paste †. *Nanoscale* **2018**, *10*, 1004. https://doi.org/10.1039/c7nr07561h.
- (54) Yao, Y.; Lin, Z.; Lin, Z.; Song, X.; Moon, K. S.; Wong, C. P. Large-Scale Production of Two-Dimensional Nanosheets. *J. Mater. Chem.* 2012, 22 (27), 13494–13499. https://doi.org/10.1039/c2jm30587a.
- (55) Zheng, X.; Wang, G.; Huang, F.; Liu, H.; Gong, C.; Wen, S.; Hu, Y.; Zheng, G.; Chen, D. Liquid Phase Exfoliated Hexagonal Boron Nitride/Graphene Heterostructure Based Electrode Toward Asymmetric Supercapacitor Application. *Front. Chem.* **2019**, *7*, 544. https://doi.org/10.3389/fchem.2019.00544.
- (56) Wang, H.; Su, X.; Song, T.; Li, Z.; Zhao, Y.; Lou, H.; Wang, J. Scalable Exfoliation and Dispersion of Few-Layer Hexagonal Boron Nitride Nanosheets in NMP-Salt Solutions. *Appl. Surf. Sci.* **2019**, *488*, 656–661. https://doi.org/10.1016/j.apsusc.2019.05.296.
- (57) Wang, N.; Yang, G.; Wang, H.; Yan, C.; Sun, R.; Wong, C. P. A Universal Method for Large-Yield and High-Concentration Exfoliation of Two-Dimensional Hexagonal Boron Nitride Nanosheets. *Mater. Today* **2019**, *27*, 33–42. https://doi.org/10.1016/j.mattod.2018.10.039.
- (58) Li, X.; Hao, X.; Zhao, M.; Wu, Y.; Yang, J.; Tian, Y.; Qian, G. Exfoliation of Hexagonal Boron Nitride by Molten Hydroxides. *Adv. Mater.* **2013**, *25* (15), 2200–2204. https://doi.org/10.1002/adma.201204031.
- (59) Donato, M. G.; Messina, E.; Foti, A.; Smart, T. J.; Jones, P. H.; Iatì, M. A.; Saija, R.;

- Gucciardi, P. G.; Maragò, O. M. Optical Trapping and Optical Force Positioning of Two-Dimensional Materials. *Nanoscale* **2018**, *10* (3), 1245–1255. https://doi.org/10.1039/c7nr06465a.
- (60) Moore, V. C.; Strano, M. S.; Haroz, E. H.; Hauge, R. H.; Smalley, R. E.; Schmidt, J.; Talmon, Y. Individually Suspended Single-Walled Carbon Nanotubes in Various Surfactants. *Nano Lett.* 2003, 3 (10), 1379–1382. https://doi.org/10.1021/nl034524j.
- (61) Smith McWilliams, A. D.; de los Reyes, C. A.; Liberman, L.; Ergülen, S.; Talmon, Y.; Pasquali, M.; Martí, A. A. Surfactant-Assisted Individualization and Dispersion of Boron Nitride Nanotubes. *Nanoscale Adv.* **2019**, *1* (3), 1096–1103. https://doi.org/10.1039/c8na00315g.
- (62) Smith, R. J.; Lotya, M.; Coleman, J. N. The Importance of Repulsive Potential Barriers for the Dispersion of Graphene Using Surfactants. *New J. Phys.* **2010**, *12*, 125008. https://doi.org/10.1088/1367-2630/12/12/125008.
- (63) Bellare, J. R.; Davis, H. T.; Scriven, L. E.; Talmon, Y. Controlled Environment Vitrification System: An Improved Sample Preparation Technique. *J. Electron Microsc. Tech.* **1988**, *10* (1), 87–111. https://doi.org/10.1002/jemt.1060100111.
- (64) Lotya, M.; King, P. J.; Khan, U.; De, S.; Coleman, J. N. High-Concentration, Surfactant-Stabilized Graphene Dispersions. *ACS Nano* **2010**, *4* (6), 3155–3162. https://doi.org/10.1021/nn1005304.
- (65) Lotya, M.; Hernandez, Y.; King, P. J.; Smith, R. J.; Nicolosi, V.; Karlsson, L. S.; Blighe, F. M.; De, S.; Zhiming, W.; McGovern, I. T.; Duesberg, G. S.; Coleman, J. N. Liquid Phase Production of Graphene by Exfoliation of Graphite in Surfactant/Water Solutions. *J. Am. Chem. Soc.* **2009**, *131* (10), 3611–3620. https://doi.org/10.1021/ja807449u.
- (66) Dorn, R. W.; Ryan, M. J.; Kim, T.-H.; Goh, T. W.; Venkatesh, A.; Heintz, P. M.; Zhou, L.; Huang, W.; Rossini, A. J. Identifying the Molecular Edge Termination of Exfoliated Hexagonal Boron Nitride Nanosheets with Solid-State NMR Spectroscopy and Plane-Wave DFT Calculations. *Chem. Mater.* 2020, 32 (7), 3109–3121. https://doi.org/10.1021/acs.chemmater.0c00104.
- (67) Di Meo, E. M.; Di Crescenzo, A.; Velluto, D.; O'Neil, C. P.; Demurtas, D.; Hubbell, J. A.; Fontana, A. Assessing the Role of Polyethylene Glycol-Bl-Propylene Sulfide (PEG-PPS) Block Copolymers in the Preparation of Carbon Nanotube Biocompatible Dispersions. *Macromolecules* 2010, 43 (7), 3429–3437. https://doi.org/10.1021/ma902443j.
- (68) Lu, F.; Wang, F.; Gao, W.; Huang, X.; Zhang, X.; Li, Y. Aqueous Soluble Boron Nitride Nanosheets via Anionic Compound-Assisted Exfoliation. *Mater. Express* **2013**, *3* (2), 144–150. https://doi.org/10.1166/mex.2013.1110.
- (69) Pandit, S.; Gaska, K.; Mokkapati, V. R. S. S.; Forsberg, S.; Svensson, M.; Kádár, R.; Mijakovic, I. Antibacterial Effect of Boron Nitride Flakes with Controlled Orientation in Polymer Composites. RSC Adv. 2019, 9 (57), 33454–33459. https://doi.org/10.1039/c9ra06773f.
- (70) Davesne, A. L.; Lazar, S.; Bellayer, S.; Qin, S.; Grunlan, J. C.; Bourbigot, S.; Jimenez, M. Hexagonal Boron Nitride Platelet-Based Nanocoating for Fire Protection. *ACS Appl. Nano Mater.* **2019**, *2* (9), 5450–5459. https://doi.org/10.1021/acsanm.9b01055.

ASSOCIATED CONTENT Supporting Information Available: Optimization of the dispersion procedure in sodium cholate, TGA confirmation of the surfactant removal, images of the dispersions and demonstration of the Tyndall effect, XPS of hBN, AFM images of hBN dispersions after 100g centrifugation, supplementary AFM images of hBN dispersions after 8000g centrifugation, histograms of the hBN sheet thickness and lateral width in dispersions after 8000g centrifugation, supplementary cryo-TEM images, and AFM images of dispersions after 24 days.

# For Table of Contents only:

